Earthquake Geotechnical Engineering for Protection and Development of Environment and Constructions – Silvestri & Moraci (Eds)
© 2019 Associazione Geotecnica Italiana, Rome, Italy, ISBN 978-0-367-14328-2

Physical modelling of anchored steel sheet pile walls under seismic actions

A. Fusco, G.M.B. Viggiani & S.P.G. Madabhushi
University of Cambridge, Cambridge, UK

G. Caputo & R. Conti
Università Niccolò Cusano, Rome, Italy

C. Prüm
ArcelorMittal, Luxemburg, Luxemburg

ABSTRACT: This paper describes an experimental investigation of the behaviour of anchored Steel Sheet Pile (SSP) walls under seismic actions. Dynamic centrifuge tests on reduced scale models of anchored SSP walls in dry medium dense sand were carried out on the Turner beam centrifuge at the Schofield Centre, Cambridge University. In order to be able to observe the failure mechanism, the tests were carried out in a rigid container with a Perspex viewing window. A layer of Duxseal© was placed on the lateral boundaries of the container to minimise reflections. The amplitude of the earthquakes was increased up to a peak acceleration significantly higher than critical, in order to trigger failure of the soil-wall-anchor system. In this paper the experimental results are presented in terms of bending moments along the retaining wall, anchor forces and displacement fields of both the retaining wall and the soil behind it. Displacement field and hence soil strains were obtained by particle image velocimetry analyses.

1 INTRODUCTION

Anchored Steel Sheet Pile (SSP) walls are frequently adopted as retaining structures in port facilities, as they may be more economical and easier to install than gravity or semi-gravity cantilevered walls. In current design practice, anchored SSP walls are usually designed employing simple methods based on the limit analysis or on limit equilibrium solutions, in which the seismic actions are introduced as equivalent static forces (pseudo-static approach) and the performance of the system is quantified in terms of a static safety factor against an assumed failure mechanism (PIANC 2001). In highly seismic areas, however, this simple approach may lead to over-conservative and uneconomical design. In principle, more cost-effective design may be achieved using numerical analyses carried out by finite element or finite difference methods. However, to get sensible results from numerical analyses, several factors need to be evaluated carefully including *e.g.*, the selection of representative acceleration time histories and boundary conditions, and an appropriate constitutive model for the soil. Moreover, fully coupled dynamic numerical modelling of geotechnical systems is very demanding from the computational point of view and, hence, not always easily accessible to the practicing engineer.

In recent years, increasing attention has been given to performance-based design and simplified displacement methods. In performance-based design, it is accepted that the strength of a ductile retaining system may be exceeded during the earthquake and, therefore, that the structure may accumulate permanent displacements, provided they are smaller than some acceptable value. Design can still be formally carried out as capacity based, *i.e.*, evaluating a pseudo-

static safety factor against an assumed failure mechanism, but this would be computed adopting a conventionally reduced value of the seismic coefficient that depends on the acceptable permanent displacement. Newmark's sliding block method is usually employed to estimate the permanent displacement experienced by gravity and cantilevered retaining walls under a given earthquake (Zeng & Steedman 2000, Conti et al. 2013).

A key ingredient for the application of simplified displacement methods is the evaluation of the critical acceleration, a_c, which is the acceleration that fully mobilizes the resistance of the system and is typically obtained by limit analysis or limit equilibrium methods. For anchored SSP walls, several failure mechanisms are possible. Depending on the system layout and the relative strength of the system components, these may correspond to local and global soil failure mechanisms, anchor failure and failure of the structural members. The critical acceleration should be obtained as the minimum value of acceleration corresponding to the activation of any potential failure mechanism.

Identifying the failure mechanisms actually occurring in the anchor-soil-retaining wall system is necessary to extend successfully the Newmark's approach to the prediction of permanent displacements for this type of anchored SSP walls. Centrifuge modelling represents a powerful tool to address this problem, since the correct failure mechanism in a boundary value problem can be observed at the correct stress level. This paper presents some preliminary results of an experimental programme including four centrifuge tests on reduced scale models of anchored SSP walls in dry medium dense sand. Particle Image Velocimetry (PIV) was employed to compute the displacement field and the shear strain in the soil around the anchor and the main wall. The experimental evidence on the behaviour of anchored SSP walls under seismic actions will be used to validate simplified solutions adopted to calculate the critical accelerations and the displacements of the wall and, possibly, to validate numerical methods.

2 EXPERIMENTAL LAYOUT

The experimental program was carried out on the Turner beam centrifuge at the Schofield Centre, University of Cambridge. Figure 1 defines the main geometrical parameters for an anchored SSP wall and Table 1 summarises the dimensions of the four centrifuge models, which were carried out at an increased gravity of 60*g*.

2.1 *Materials and instrumentation*

The small-scale models of the main retaining wall and of the anchor wall were made using 4.7 mm thick aluminium plates, with the same bending stiffness of an AZ28 profile at prototype scale. The main wall was instrumented with six full Wheatstone bridge strain gauges to measure the bending moments along its height. Four Micro-Electrical-Mechanical Systems (MEMS) accelerometers were used to measure the horizontal acceleration at mid height and

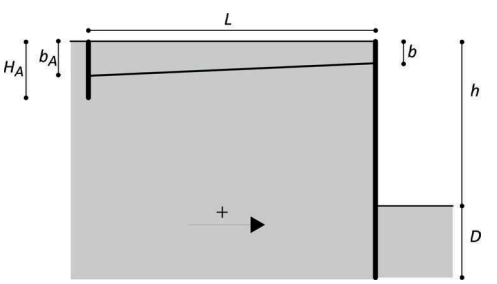

Figure 1. Layout of an anchored SSP wall. The arrow indicates the direction of positive accelerations.

Table 1. Experimental programme, dimensions at prototype scale.

	Dimensions [m]					
Test ID	h	D	b	b_A	H_A	L
AF02	7	3	0.5	0.5	2	17
AF03	8	2	0.5	0.5	2	17
AF04	8	2	0.5	1.3	2	12
AF05	8	2	0.5	0.5	2	12

at the top of the main wall (two at the top, two at mid height). Transparent plastic strips were attached to the sides of the two walls to prevent sand particles from flowing through the gap between the wall ends and the box, which would alter plain strain conditions due to friction given by sand particles stuck between the sides of the container and the sides of the two walls.

Four tie-backs were realized employing steel cables instrumented with load cells, to measure the anchor forces. The connection between the cables and the retaining wall was obtained by passing the cables through holes in the aluminium plate and fixing their ends with aluminium cylinders, to obtain a hinged connection. Cylindrical hinges were manufactured to connect the cables to the anchor wall.

The soil was Hostun sand (G_S = 2.65, e_{max} = 1.011, e_{min} = 0.555, ϕ_{cv} = 33°). The target relative density, D_r = 50%, was achieved using an automatic sand pourer available at the Schofield Centre. Fourteen piezoelectric accelerometers were placed in the sand to measure the horizontal acceleration at different locations within the soil layer and one Linear Variable Differential Transducer (LVDT) was used to measure the settlement of the soil surface immediately behind the retaining wall. Two piezoelectric accelerometers were placed on the external side of the box to measure the input motion. Figure 2 shows a cross section of the model and the layout of the instrumentation adopted for test AF04.

2.2 *The container*

The four centrifuge tests were carried out in a rigid box with absorbing boundaries. The internal dimensions of the container are $W \times H \times D$ = 500×360×250 mm^3 and a 25 mm layer of Duxseal© was used to minimise energy reflections at the boundaries (Steedman & Madabhushi 1991). The box has a perspex front viewing window, allowing soil deformations and wall displacements to be measured during the tests by PIV. Images of the cross section of the model were taken employing a high-speed camera, able of recording up to 1000 frames per second, placed on a gantry in front of the window. The images were analysed using the Matlab-based software GeoPIV-RG (Stainer et al. 2015).

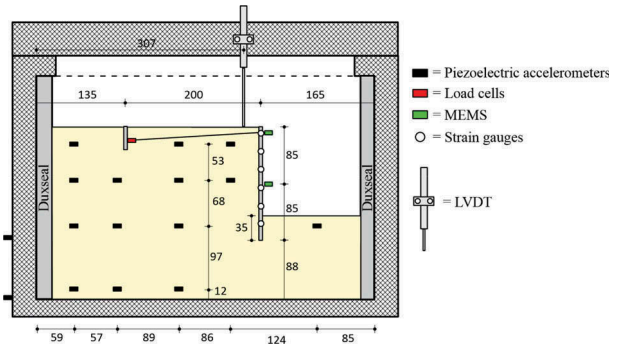

Figure 2. Layout of instrumentation in test AF04 (dimensions in mm).

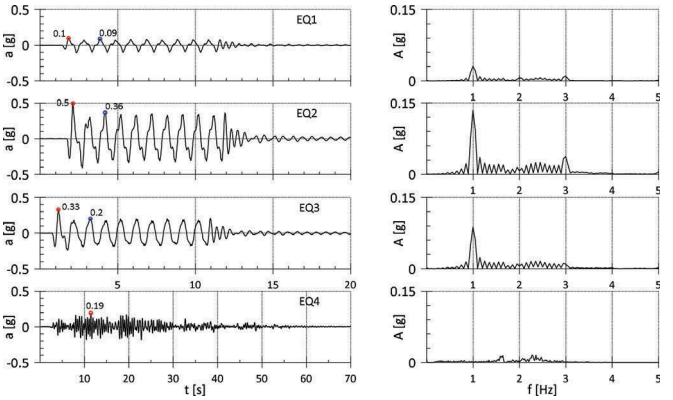

Figure 3. Input acceleration time histories and amplitude Fourier spectra (prototype scale).

2.3 *Input motion*

Figure 3 shows the acceleration time histories and the Fourier amplitude spectra of the four earthquakes applied during test AF04. The input motions consisted of three trains of 10 nearly sinusoidal cycles with different peak accelerations and the same main frequency, f_m = 1 Hz, and one acceleration time history recorded during the Imperial Valley earthquake (dominant frequency of 2.27 Hz). These were applied to the models using a servo-hydraulic actuator (Madabhushi et al. 2012). For the trains of sinusoidal waves, the first peak is always slightly above the target value, which was chosen to be smaller, larger and about the same as the critical acceleration for the soil-wall-anchor system evaluated using the limit equilibrium solution proposed by Caputo et al. (2019) for a global failure mechanism ($a_c = 0.15g$). In the following, positive accelerations are directed towards the retaining wall (see Figure 1).

3 EXPERIMENTAL OBSERVATIONS

3.1 *Measurements from instrumentation placed on the model*

For the sake of brevity, only the results of test AF04 are shown in the following. Unless otherwise stated, all results are given at prototype scale.

Figures 4(a) to (d) show the input acceleration time history for EQ2, together with the horizontal surface accelerations measured in free-field conditions on the left of the anchor wall (see Figure 1), at mid-height, and at the top of the retaining wall. A very slight amplification of the input signal is observed in the free-field, with a ratio of maximum acceleration at surface to input acceleration equal to only 1.16, whereas amplification phenomena become more relevant at mid-height (acceleration ratio 1.22) and at the top (acceleration ratio 1.41) of the wall.

Figure 4(e) shows the time history of the force measured in the tie-backs. This is given as tie-back force per unit length, and has been computed by taking the sum of the forces measured by the four load cells and dividing it by the length of the retaining wall. As expected, for positive accelerations (rightward, in the chosen reference system), the tie-back forces drop, because the inertial forces are leftward, reducing the thrust on the retaining structure. Some residual increase of tie-back force was always recorded at the end of each earthquake; in this case the tie-back force increased from 55 kN/m to 59 kN/m, by about 7%.

Figure 4(f) shows the vertical displacement measured at surface by the LVDT placed immediately behind the retaining wall. Significant settlements were experienced by the backfill, due to both soil densification and outward displacement of the retaining wall, as discussed in more detail in the following.

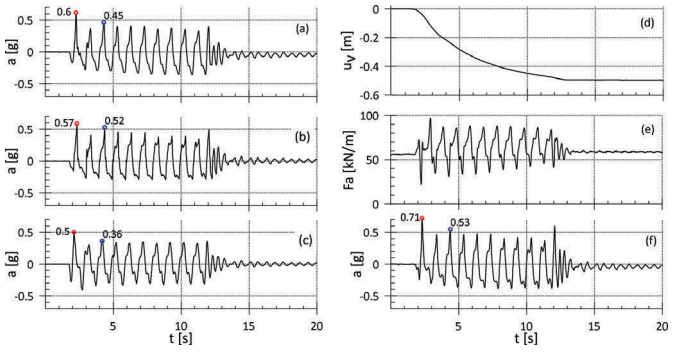

Figure 4. EQ2. Acceleration time histories: (a) wall mid-height, (b) soil surface, (c) input acceleration, (f) wall top, and (e) tie-back force and (d) vertical displacements at surface.

Figure 5(a) and (b) show the envelopes of the maximum measured bending moment during each earthquake and the profiles of residual bending moment after each earthquake, respectively. In both cases, these are compared with the profile of bending moment measured right at the end of the spin up (static). The maximum residual increment of bending moment after the earthquakes is of the order of 45 KNm/m or 25% of the static value, consistently with data from other Authors (Zeng & Steedman 1993, Madabhushi & Zeng 2007). According to Whitman (1990) and Zeng (1990), residual bending moments and anchor forces are related to the sand densification under seismic shaking, which implies that the horizontal stress are "locked" behind the retaining wall after each earthquake (Conti 2012).

3.2 *Displacements of retaining wall and anchor wall*

Figure 6 shows the displacements of the retaining wall and of the anchor wall after EQ1 and EQ2, as obtained by PIV. The displacements of the wall did not increase significantly after the following two earthquakes (EQ3 and EQ4). At the end of EQ1, the horizontal displacement of top of the wall is about 0.08 m, whereas the displacement at the toe is nearly null. After EQ2, the horizontal displacement of the top of the wall increased to about 0.69 m, and the toe displaced by about 0.08 m, corresponding to an outward rotation of 6.1%. The horizontal displacements of the anchor wall are similar in magnitude to those of the main wall, but the wall remains nearly vertical at the end of EQ1 and experiences only a very small counter clockwise rotation, of the order of 1.7%, at the end of EQ2, consistently with the fact that the tie-backs are connected to the anchor wall at 1/3 of its height.

Figure 7(a) and (b) show, for earthquake EQ2, the time histories of the incremental horizontal displacements (i.e., the displacements recorded during EQ2 minus those at the end of

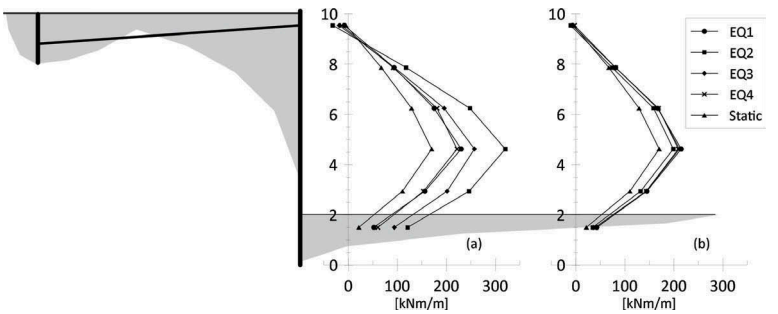

Figure 5. Bending moments: (a) maximum, (b) residual.

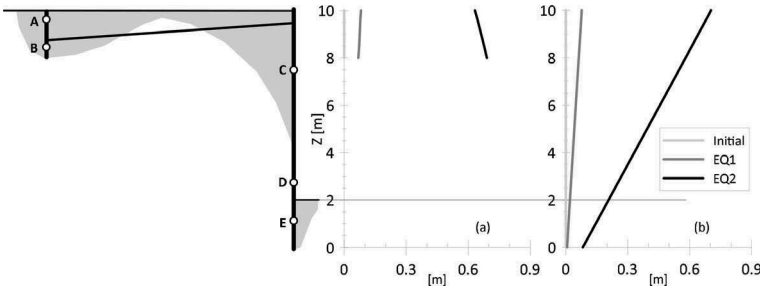

Figure 6. Horizontal displacements of: (a) anchor wall and (b) retaining wall after EQ1 and EQ2.

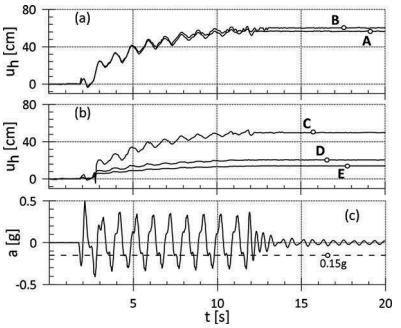

Figure 7. EQ2 – incremental horizontal displacements of points of: (a) main wall and (b) anchor wall and (c) input acceleration time history.

EQ1) of three points on the main wall and two points on the anchor wall, respectively. The locations of these points are given in Figure 6. The data in Figure 7 are consistent with the kinematics in Figure 6, in that the incremental displacements of points A and B, on the anchor wall, are nearly the same, indicating a horizontal translation, whereas the displacements of point C towards the top of the main wall, are much larger than those of points D and E, towards the wall toe, indicating a significant rotation.

Figure 7(c) shows the input acceleration time history for EQ2, together with the theoretical value of the critical acceleration of the system. As expected, the wall accumulates permanent displacements every time the input acceleration exceeds the critical value (note that negative accelerations correspond to inertia forces directed towards the wall). However, even if the amount by which and the time over which the input acceleration remains above threshold are the same in each cycle, the incremental permanent displacements progressively reduce, indicating that the strength of the system increases with time. This is possibly due to densification of the backfill (Zeng 1990) and to progressive mobilization of passive resistance in front of the anchor wall and the retaining wall (Conti et al. 2012).

The increase of critical acceleration also explains why the retaining wall did not move further during the last two earthquakes.

3.3 *Failure mechanism*

Figure 8(a) is an image of model AF04, showing the grid of reference dots used to calibrate PIV. Figure 8(b) shows the displacement vectors in the soil obtained at the end of EQ2. Near the surface, the horizontal component of the displacement vectors is nearly constant between the anchor wall and the main wall, whereas the vertical components of the displacement vectors increase significantly immediately behind the main wall. Incidentally, the value of vertical

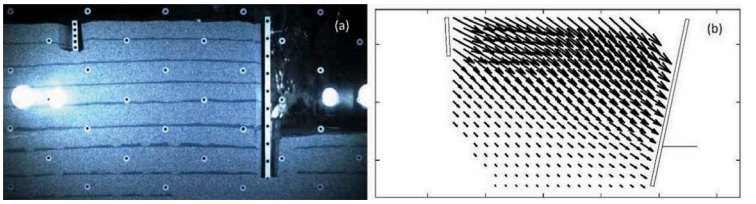

Figure 8. EQ2 – (a) image of model and (b) displacement vectors as computed by PIV

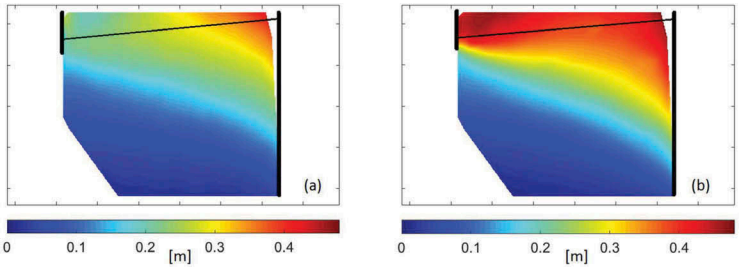

Figure 9. EQ2 – contours of (a) vertical and (b) horizontal displacements in the soil

displacement behind the wall obtained by PIV (≈ 0.5 m) matches very closely that measured directly using the LVDT (≈ 0.5 m). This pattern is confirmed by the contours of vertical and horizontal displacements in Figure 9(a) and (b), respectively, which also indicate quite clearly the extent of the wedge of soil involved in the failure mechanism. This is delimited laterally by the two walls and at the bottom by a surface extending from the bottom of the anchor wall to some point close to the top of the embedded portion of the main wall.

The progressive development of the shear surface with cycling is clearly identified in Figure 10(a) and (b) showing the shear strain contours after 5 cycles and at the end of EQ2, respectively. The shape of the shear surface identified by PIV is consistent with the global mechanism predicted by limit equilibrium for this layout. After 5 cycles of shaking, a strain concentration occurs immediately in front of the anchor wall and at the back of the upper portion of the main wall, possibly corresponding to the development of passive and active

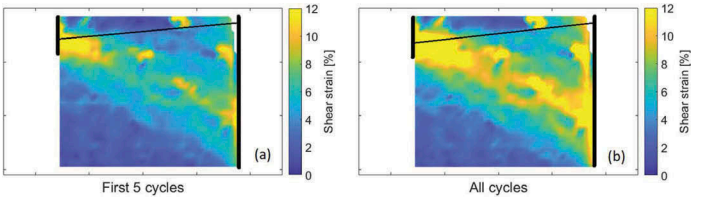

Figure 10. Contours of shear strain in the soil (a) after 5 cycles of and (b) at the end of EQ2

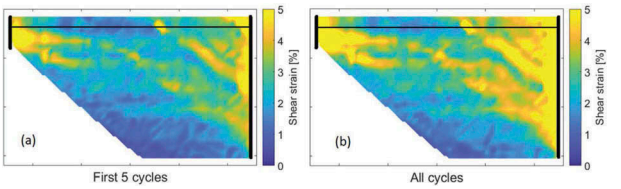

Figure 11. Test AF03: Contours of shear strain in the soil (a) after 5 cycles of and (b) at the end of EQ3

wedges. However, at the end of the shaking, the shear strains along the global failure surface eventually coalesce, as the global mechanism is fully activated.

This occurs also for test AF05, with a relatively small distance between the anchor wall and the main wall, whereas, for other layouts, such as AF02 and AF03, characterised by larger distances between the anchor wall and the main wall, the strains along a potential global failure surface do not coalesce and eventually local passive and active failure mechanisms develop in front of the anchor and at the back of the wall, see Figure 11.

4 CONCLUSIONS

Four dynamic centrifuge tests were carried out on small-scale models of anchored SSP retaining walls in medium dense dry sand to examine their behaviour under seismic actions with accelerations larger than the critical acceleration computed by limit equilibrium methods. For the examined layouts, the critical failure mechanism corresponded to local failure of the soil in front of the anchor or global failure of the system along a shear surface connecting the anchor and the main retaining wall. The failure mechanisms were revealed very clearly by the displacement and strain fields reconstructed by PIV analyses. The walls accumulated permanent displacements when the input acceleration exceeded the critical value, but the incremental permanent displacements in each successive cycle reduced, indicating that the strength of the system increases with time, possibly due to densification of the backfill and to progressive mobilization of passive resistance in front of the anchor wall and retaining wall.

ACKNOWLEDGEMENT

The project leading to this application has received funding from the European Union's Horizon 2020 research and innovation programme under grant agreement No 730900.

REFERENCES

Caputo, G., Conti, R., Viggiani, G.M.B., & Prüm, C. Theoretical framework for the seismic design of anchored steel sheet pile walls. In *Proceedings of the 7th International Conference on Earthquake Geotechnical Engineering, ICEGE*, 2019.

Conti, R., Madabhushi, G. S. P., & Viggiani, G. M. B. (2012). On the behaviour of flexible retaining walls under seismic actions. *Géotechnique*, 62(12), 1081.

Conti, R., Viggiani, G. M., & Cavallo, S. (2013). A two-rigid block model for sliding gravity retaining walls. *Soil Dynamics and Earthquake Engineering*, 55, 33–43.

International Navigation Association. PIANC. (2001). Seismic Design Guidelines for Port Structures.

Madabhushi, G. S., Haigh, S. K., Houghton, N. E., & Gould, E. (2012). Development of a servo-hydraulic earthquake actuator for the Cambridge Turner beam centrifuge. *International Journal of Physical Modelling in Geotechnics*, 12(2), 77–88.

Madabhushi, S. P. G., & Zeng, X. (2007). Simulating seismic response of cantilever retaining walls. *Journal of Geotechnical and Geoenvironmental Engineering* 133(5), 539–549.

Stanier, S. A., Blaber, J., Take, W. A., & White, D. J. (2015). Improved image-based deformation measurement for geotechnical applications. *Canadian Geotechnical Journal*, 53(5), 727–739.

Steedman, R. S., & Madabhushi, S. P. G. (1991). Wave transmission at a multi-media interface. In *Proceedings of the 5th International Conference on Soil Dynamics and Earthquake Engineering. Elsevier*.

Whitman, R. V. (1990). Seismic design and behaviour of gravity retaining walls. In Design and performance of earth retaining structures (eds P. Lambe and L. A. Hansen), *Geotechnical Special Publication* No. 25, pp. 817–842. Reston, VA, USA: ASCE.

Zeng, X. (1990). Modelling the behaviour of quay walls in earthquakes. PhD thesis, University of Cambridge, UK.

Zeng, X. & Steedman, R. S. (1993). On the behaviour of quay walls in earthquakes. *Géotechnique* 43, No. 3, 417–431.

Zeng, X., & Steedman, R. S. (2000). Rotating block method for seismic displacement of gravity walls. *Journal of Geotechnical and Geoenvironmental Engineering*,126(8), 709–717.